Published in final edited form as:

Cancer Res. 2020 January 15; 80(2): 156–162. doi:10.1158/0008-5472.CAN-19-0201.

Photodynamic Therapy Is an Effective Adjuvant Therapy for Image-Guided Surgery in Prostate Cancer

Xinning Wang[1], **Gopolakrishnan Ramamurthy**[2], **Aditi A. Shirke**[1], **Ethan Walker**[1], **Joey Mangadlao**[2], **Ziying Wang**[1], **Yu Wang**[2], **Lingpeng Shan**[3], **Mark D. Schluchter**[3], **Zhipeng Dong**[4], **Susann M. Brady-Kalnay**[5], **Natalie K. Walker**[6], **Madhusudhana Gargesha**[7], **Gregory MacLennan**[8], **Dong Luo**[2], **Rongcan Sun**[9], **Bryan Scott**[7], **Debashish Roy**[7], **Jing Li**[10], **James P. Basilion**[1,2]

[1]Department of Biomedical Engineering, Case Western Reserve University, Cleveland, Ohio.

[2]Department of Radiology, Case Western Reserve University, Cleveland, Ohio.

[3]Department of Population and Quantitative Health Sciences, Case Western Reserve University, Cleveland, Ohio.

[4]Department of Mechanical Engineering, Case Western Reserve University, Cleveland, Ohio.

[5]Department of Molecular Biology and Micro Biology, Case Western Reserve University, Cleveland, Ohio.

[6]Lerner College of Medicine, Cleveland Clinic, Cleveland, Ohio.

[7]BioInvision Inc., Mayfield Village, Ohio.

[8]Department of Pathology and Urology, University Hospitals Cleveland Medical Center, Case Western Reserve University, Cleveland, Ohio.

[9]Department of Biochemistry, Case Western Reserve University, Cleveland, Ohio.

[10]Department of Chemistry, Case Western Reserve University, Cleveland, Ohio.

Corresponding Authors: James P. Basilion, Case Western Reserve University, 11100 Euclid Ave, Wearn Building B-42, Cleveland, OH 44106-5056. Phone: 216-983-3246; Fax: 216-844-4987,: james.basilion@case.edu; and Xinning Wang, Department of Biomedical Engineering, Case Western Reserve University, 11100 Euclid Ave, Wearn Building B-49, Cleveland, OH 44106-5056. Phone: 216-983-3254; Fax: 216-844-4987, xxw171@case.edu.

Authors' Contributions

Conception and design: X. Wang, M.D. Schluchter, J.P. Basilion

Development of methodology: X. Wang, G. Ramamurthy, E. Walker, J. Mangadlao, J.P. Basilion

Acquisition of data (provided animals, acquired and managed patients, provided facilities, etc.): X. Wang, A.A. Shirke, E. Walker, J. Mangadlao, Y. Wang, Z. Dong, N.K. Walker, D. Luo, J. Li

Analysis and interpretation of data (e.g., statistical analysis, biostatistics, computational analysis): X. Wang, A.A. Shirke, E. Walker, Z. Wang, L. Shan, M.D. Schluchter, Z. Dong, M. Gargesha, G. MacLennan, B. Scott, D. Roy, J.P. Basilion

Writing, review, and/or revision of the manuscript: X. Wang, E. Walker, N.K. Walker, J.P. Basilion

Administrative, technical, or material support (i.e., reporting or organizing data, constructing databases): X. Wang, G. Ramamurthy, M. Gargesha, R. Sun, B. Scott, D. Roy, J.P. Basilion

Study supervision: X. Wang, J.P. Basilion

Other (Model Development): S.M. Brady-Kalnay

Supplementary data for this article are available at Cancer Research Online (http://cancerres.aacrjournals.org/).

Disclosure of Potential Conflicts of Interest

X. Wang has an unpaid consultant/advisory board relationship with Exotome. J.P. Basilion is a consultant at Akrotome Imaging and Vergent Biosciences, reports receiving other commercial research support from Akrotome, and has an ownership interest (including patents) in Exotome LLC, Akrotome, and Vergent Biosciences. No potential conflicts of interest were disclosed by the other authors.

Abstract

Local and metastatic relapses of prostate cancer often occur following attempted curative resection of the primary tumor, and up to 66% of local recurrences are associated with positive margins. Therefore, technologies that can improve the visualization of tumor margins and adjuvant therapies to ablate remaining tumor tissues are needed during surgical resection of prostate adenocarcinoma. Photodynamic agents have the potential to combine both fluorescence for image-guided surgery (IGS) and photodynamic therapy (PDT) to resect and ablate cancer cells. The objective of this study was to determine the utility of a targeted PDT agent for IGS and adjuvant PDT. Using a previously developed prostate-specific membrane antigen (PSMA)–targeted PDT agent, PSMA-1-Pc413, we showed that PSMA-1-Pc413 selectively highlighted PSMA-expressing tumors, allowing IGS and more complete tumor resection compared with white light surgery. Subsequent PDT further reduced tumor recurrence and extended animal survival significantly. This approach also enabled identification of tumor cells in lymph nodes. In summary, this study presents a potential new treatment option for patients with prostate cancer undergoing surgery, which improves tumor visualization and discrimination during surgery, including identification of cancer in lymph nodes.

Significance: These findings present a photodynamic agent that can be used for both photodynamic therapy and image-guided surgery, allowing better visualization of tumor margins and elimination of residual tumor tissues.

Introduction

Prostate cancer is the most prevalent cancer among men in the United States and is their second leading cause of cancer death (1). Prostatectomy and radiotherapy have been the mainstay treatment for men with localized prostate cancer. However, wide variations in the incidence of positive surgical margins (11%–48%) have been reported at the time of radical prostatectomy (2) and have been repeatedly demonstrated to be associated with greater rates of biochemical (3) and local recurrence (4). Achieving a negative surgical margin may be an opportunity for the surgeon to improve surgical impact on the disease.

Surgeons predominantly use visual examination and palpation during surgery to determine the extent of the tissues to be removed; however, these are insufficient to confirm all tumor sites, particularly for some nonpalpable and invisible occult tumors (5). Adjuvant radiotherapy and chemotherapy often result in failure to halt disease and are associated with severe side effects (6), and there is an urgent need for better approaches. To fill this need, fluorescent image-guided surgery (IGS) is being developed (5), which, compared with white light surgery (WLS), can identify cancerous tissue, delineate tumor margins, and potentially reduce damage to important normal structures.

Photodynamic therapy (PDT) is a treatment that uses a photosensitizer (PS) and activation by a particular wavelength of light (7), which will produce reactive oxygen species (ROS) that kill nearby cells. Because PS are also fluorescent, they can also serve as a source for image contrast, i.e., theranostic (8). Recently, targeted PDT agents are under development or in clinical trials, without surgery, for head and neck cancers (9, 10). We have developed prostate-specific membrane antigen (PSMA)–targeted PDT agents, including

PSMA-1-Pc413 (11). PSMA-1-Pc413 strongly emits near-IR (NIR) light at 678 nm, binds to PSMA-expressing cancer cells, and is able to destroy them when irradiated by NIR light (11). Due to limitations in light penetration and irradiating all tumor cells, we postulated that it might be more effective to use PSMA-1-Pc413 as a theranostic combining IGS and PDT to fully ablate nonresected tumor tissues and/or cancer cells. Currently, there are very few examples of IGS followed by PDT, and most of these studies rely on nonspecific or nontargeted uptake of PDT agents into the tumor, e.g., 5-ALA for glioblastoma (12). No such study has been performed on prostate cancer. In this study, we used PSMA-targeted Pc413 for IGS followed by PDT (Fig. 1A) and found that PSMA-1-Pc413 was able to visualize cancer, enable more complete surgery, and effectively destroy invisible localized microscopic cancer cells (13) by PDT.

Materials and Methods

Cell culture

Retrovirally transfected PSMA-positive PC3pip cells were obtained from Dr. Michel Sadelain (Memorial-Sloan Kettering Cancer Center, New York, NY). CWR22vr1 cells were obtained from the ATCC. Cells were last checked by Western blot and flow sorted in 2018, and no genetic authentication was performed. *Mycoplasma* test was last performed in 2015. Cells were maintained in RPMI1640 medium with 10% FBS. PC3pip cells were transfected with GFP by lentivirus infection. Cells were discarded after passage 6.

Detection of ROS *in vivo*

Animal experiments were approved by the University Institutional Animal Care and Use Committee (#150033).

Six- to 8-week-old male athymic nude mice were implanted subcutaneously with 1×10^6 of PC3pip on the right dorsum. When tumor diameter reached 10 mm, PSMA-1-Pc413 (0.5 mg/kg) was injected i.v. via the tail vein. Twenty-four hours later, mice received 100 nmol of ROSstar800cw (Li-Cor Biosciences) in PBS. Animals were imaged 30 minutes later and then illuminated with 672 nm laser (Applied Optronics Corp) with irradiance of 33.3 mW/cm^2 for 25 minutes (total radiant exposure of 150 J/cm^2). Fluorescence imaging was performed on a Maestro *In Vivo* Imaging system (Perkin-Elmer): yellow filter for PSMA-1-Pc413 signal (excitation 575–605 nm, emission filter 645 nm longpass); deep red filter for ROSstar800cw (excitation 671–705 nm, emission filter 750 nm longpass). Experiments were repeated in 3 mice.

Detection sensitivity for PSMA-1-Pc413

PSMA-1-Pc413 and Forte700 NHS ester (Curadel LLC) were serially diluted in mouse serum and taken up by microcapillary tubes. The tubes were inserted to a cap device with 10 μL sample volume window (Curadel LLC) and imaged at 700 nm (Curadel RP1 Fluorescence Image System) using 100% power and varying exposure. Signals from each capillary tube were quantified using Curadel software.

In vivo image of PSMA-1-Pc413 in orthotopic mice model

To establish an orthotopic prostate cancer model (14), 6- to 8-week-old athymic nude mice were first anesthetized by i.p. injection of 50 mg/kg ketamine/xylazine. A transverse incision was made in the lower abdomen to expose the prostate. Ten microliters of PC3pipGFP cells (5×10^5) in PBS were injected into the dorsal lateral prostate gland. The incision in the abdominal wall was then closed. After about 4 weeks (tumor diameter approximately 1 cm), mice receive 0.5 mg/kg PSMA-1-Pc413 and were imaged 24 hours later by a Maestro imaging device (yellow filter: PSMA-1-Pc413, excitation 575–605 nm, emission filter 645 nm longpass; and blue filter: GFP, excitation 445–490 nm, emission filter 515 nm longpass). Mice were then euthanized. After the primary tumor was removed to expose the lymph nodes (LN) buried behind the primary tumor, the mouse was again imaged. The resected primary tumor and lymph nodes were fixed in 10% formalin, paraffin embedded, sectioned, and slides prepared. One set of the slides was subjected to hematoxylin and eosin staining, and the adjacent set was observed under a Leica DM4000B fluorescence microscope (Leica Microsystem Inc.) to visualize GFP and PSMA-1-Pc413 fluorescence. Experiments were repeated in 5 mice.

Intramuscle prostate tumor xenograft model

PSMA-positive PC3pipGFP cells (1×10^6) were injected into the muscle of the right leg of 6- to 8-week-old male athymic nude mice. Tumor growth (GFP signal) was monitored twice a week using the Maestro imaging device and calipers. When tumors reached 200 mm^3, further studies were performed.

In vivo surgery and PDT treatment of intramuscle PC3pipGFP tumors

Mice were randomly divided into three groups: WLS, IGS, and IGS, followed by PDT (IGS+PDT; Fig. 1A). All mice received 0.5 mg/kg PSMA-1-Pc413 via tail vein injection. Surgery was performed at 24 hours after injection for peak accumulation of PSMA-1-Pc413 (11). Before surgery, preimages for both GFP and PSMA-1-Pc413 were obtained. WLS was performed under room light. For IGS, tumors were removed under the guidance of Curadel RP1 at an exposure (50 ms), which allowed real-time imaging. After surgery, mice were imaged again by Maestro, and then the wounds were sutured for WLS group and IGS group. For the IGS+PDT group of animals, the resection bed was irradiated with 672 nm laser (Applied Optronics Corp) for 12.5 minutes with total radiant exposure of 75 J/cm^2 (11). Light was delivered through a GRIN-lens-terminate multimode fiber (OZ Optics) and was adjusted to cover all the surgical area (~1.0–1.5 cm in diameter). After PDT, the mice were imaged by Maestro, and the wounds were sutured. Tumor growth was then monitored by Maestro every other day for 80 days. Mice were terminated when the tumor reached the size of 1.5 cm.

Statistical analysis

The Student *t* test was used to compare Maestro signals in different treatment groups. Tumor recurrence and Kaplan–Meier survival data were analyzed by SAS9.4 using exact pairwise Wilcoxon rank-sum test. A P value < 0.05 was considered statistically significant for all comparisons.

Results

PSMA-1-Pc413 generated ROS after PDT

To confirm that PSMA-1-Pc413 generates ROS *in vivo,* its proposed mechanism of action, we used ROSstar800cw conversion into fluorescent cyanine to detect ROS (15). Before PDT, PSMA-1-Pc413 fluorescent signal was mainly observed in PC3pip tumors (Fig. 1B, top plot, 2nd and 3rd columns) with minimal ROSstar800cw fluorescence observed (Fig. 1B, bottom plot, 2nd and 3rd columns). After PDT, there was a dramatic increase in ROSstar800cw fluorescence, and little PSMA-1-Pc413 signal was observed due to photo activation (Fig. 1B, 4th column). *Ex vivo* images of the bisected tumor showed that ROS was present throughout the tumor tissues (Fig. 1B, 5th column). To assess IGS sensitivity (i.e., detection limit; ref. 16), we compared PSMA-1-Pc413 fluorescence with Forte700 NHS ester, a typical agent used to derive IGS probes (Supplementary Fig. S1). At 50 ms exposure time, the fluorescent signal from PSMA-1-Pc413 was about 2-fold higher than that from Forte700. At the highest exposure, 10 femtomol of PSMA-1-Pc413 was able to be detected (Supplementary Fig. S1C and S1D), suggesting that PSMA-1-Pc413 was suitable for IGS when imaged using the Curadel RP1 camera system.

Detection of primary tumors and LN metastasis

Most deaths from cancer are a result of metastasis. Detection of LN metastases is of major prognostic significance for many cancers. Using an orthotopic human prostate cancer mouse model, reported to develop LN metastases (17), we tested if PSMA-1-Pc413 has the ability to detect LN metastases. Twenty-four hours after PSMA-1-Pc413 administration, mice bearing orthotopic PC3pipGFP tumors displayed coincident GFP and PC413 fluorescent signals in the primary tumor (Fig. 2A). Removal of the primary tumor revealed enlarged iliac LNs as reported by others (17). Fluorescence imaging demonstrated coincidence of GFP and PSMA-1-Pc413 fluorescence in the LNs (Fig. 2A). Pathologic analysis demonstrated that both the prostate gland and LNs contained cancer and that the GFP and PSMA-1-Pc413 signals were highly correlated (Fig. 2B), demonstrating that PSMA-1-Pc413 could detect both primary prostate tumor and LN metastases.

IGS using PSMA-1-Pc413

To assess the potential utility of PSMA-1-Pc413 to aid tumor resection and ablation of remaining tumors/cancer cells, we compared animals receiving WLS, IGS, and IGS+PDT (Fig. 1A). Because mouse orthotopic prostate cancer models are not suitable for surgery, we developed an intramuscle tumor model. The muscular injection site resulted in tumors that were less encapsulated than subcutaneous xenografts, had some tissue infiltration, causing more challenges for surgery. We also demonstrated microdispersions of the cells away from the tumor mass using Cryo-imaging (Supplementary Fig. S2 and Supplementary Video S1). Twenty-four hours (11) after injection of probe, coincident fluorescent signal was observed in PC3pipGFP tumors for both GFP and PSMA-1-Pc413 (Fig. 3A and B, 2nd column). Tissue distribution at 24 hours after injection of PSMA-1-Pc413 showed highest uptake in the liver, followed by PC3pip tumor, then kidneys with washout occurring for the organs by 96 hours (Supplementary Fig. S3). Prior to surgery, the GFP and PSMA-1-Pc413 signals had similar intensities in all groups (Fig. 3C and D, left). Postoperative imaging showed

fluorescence remaining in the surgical field for WLS (Fig. 3A, 3rd column) with both GFP and PSMA-1-Pc413, and PSMA-1-Pc413 signal was detectable using the Curadel camera (Fig. 3A, bottom row). When IGS was performed, high fluorescence was observed in the tumor, which helped identify tumor tissues (Fig. 3B, bottom row; Supplementary Video S2). Minimal remaining fluorescence (GFP or PSMA-1-Pc413) was observed in mice that underwent IGS (Fig. 3B, 3rd column). Comparison of average fluorescent signals showed that both the GFP and PSMA-1-Pc413 signals (Fig. 3C and D, middle) were significantly lower in IGS and IGS+PDT groups than those in the WLS group ($P < 0.05$). These results suggest that IGS was able to highlight tumor tissue not visible during WLS, resulting in more complete tumor removal. Sequential PDT treatment of the IGS surgical wound led to significant reduction in PSMA-1-Pc413 fluorescent signal, indicating PDT was activated in the surgical bed (Fig. 3B, 4th column; Fig. 3D, right). GFP signal in the IGS wound was not significantly reduced after PDT, (Fig. 3C, right).

To demonstrate that fluorescence was associated with tumor tissues, a total of 92 pieces of both fluorescing and nonfluorescing tissues resected during IGS and IGS+PDT procedures were collected and underwent blinded pathologic analysis. Among the 92 samples, 22 did not show any fluorescence and were pathologically negative for cancer (true negatives); 68 showed fluorescence and were positive for cancer (true positives); 2 showed fluorescence, but were not cancer (false positives); and there were no false negatives. Analysis demonstrated sensitivity and specificity of 100% and 91.7%, respectively (Supplementary Table S1). Histologic and fluorescence microscopic examination of the resected tumor tissue showed that PSMA-1-Pc413 signal corresponded well with the tumor tissue (Supplementary Fig. S4), was able to delineate the borderline between cancer tissue and normal tissue, and was able to identify cancer cells that invaded into normal tissue. Taken together, these data suggest that the technology may provide precise guidance for surgery.

To further confirm that IGS will achieve more complete tumor resection, a separate set of surgeries was performed, after which, the mouse legs with surgical wounds were collected, sectioned, and examined by pathology. It was found that all 5 mice in WLS group had remaining tumor, 3 of 5 mice in IGS group had tumor, and all 4 mice in IGS+PDT group were tumor free (Supplementary Fig. S5). No damage to normal tissues was observed in the IGS+PDT wound beds following PDT (Supplementary Fig. S5).

PDT in combination with IGS reduced tumor recurrence

After surgery, we next monitored tumor recurrence (GFP signal, Supplementary Fig. S6) and animal survival to evaluate overall response to the theranostic approach. In the WLS group, residual GFP signal was observed after surgery and rapid tumor growth resulted in strong GFP signal by day 10 (Fig. 4A, 1st row). Both IGS and IGS+PDT mice showed no/minimal GFP signal after surgery (Figs. 3C and 4A). The IGS mice started to show GFP signal on day 36 after surgery (Fig. 4A and B), but no significant difference was observed in tumor recurrence between WLS and IGS mice ($P = 0.2222$). In contrast, only one mouse in the IGS+PDT group showed tumor recurrence on day 80 after surgery, and the other 7 were tumor free; significant differences were observed between IGS+PDT versus IGS ($P = 0.00084$), and IGS+PDT versus WLS ($P = 0.0008$; Fig. 4A and B). IGS

significantly extended animal survival compared with WLS ($P = 0.0317$), and IGS+PDT further prolonged animal survival to >80 days ($P = 0.0008$ compared with WLS and $P = 0.0008$ compared with IGS, Fig. 4C). No adverse effects or delay in healing was observed in IGS+PDT animals as compared with WLS and IGS animals.

We also performed studies using mice bearing prostate tumors derived from human CWR22rv1 cells, which spontaneously overexpress PSMA at a level only 1/12 of that in PC3pip cells (Supplementary Fig. S7). Despite the lower PSMA expression, the level of PSMA-1-Pc413 uptake in CWR22rv1 cells was about 50% of that in the PC3pip tumors (Supplementary Fig. S8A and S8B), and PDT effectively inhibited tumor growth without surgical intervention (Supplementary Fig. S8C). When CWR22rv1 tumors were implanted into mouse flank muscles, PSMA-1-Pc413 fluorescent signal was clearly visible and suitable for IGS (Supplementary Fig. S9). IGS+PDT again significantly delayed tumor recurrence and extended animal survival as compared with WLS and IGS groups (Supplementary Fig. S10).

Discussion

PDT has been used for selective identification and treatment of cancers. Postsurgical photoimmunotherapy (PIT) has shown inhibition of tumor recurrence after surgical resection of pancreatic (18) and head and neck cancer models (19). However, both of these did not explore the ability of PIT to aid IGS. Further, these antibody agents are significantly more expensive to make than the small urea/peptide-based agent used here, and antibody's longer circulation time could lead to off target accumulation. Although there are a few examples of IGS followed by nontargeted PDT (12), there are none for prostate cancer, which has 20% to 40% local recurrence that is associated with incomplete surgery (2, 3). Even in the few examples where IGS was followed by PDT for other cancers (12), the molecules are not as selective or designed to exploit distinct biochemical biomarkers for the disease targeted and therefore likely may have significant off-target effects and increased toxicity. We have developed a completely novel PSMA-targeted PDT agent to directly exploit overexpression of a biomarker on the surface of most prostate cancers (>95% overexpression; ref. 11). We initially tested this agent as a PDT agent only, i.e., without prior surgery, and demonstrated that primary tumors (T-stage) could be eradicated, but in all cases recurred (11). Here, we test the hypothesis that recurrence of primary tumors after PDT treatment is not complete because the tumor burden is too large for PDT to effectively "get" all the tumor cells. We hypothesized that IGS will reduce tumor burden and, followed immediately by PDT, improve survival. We showed that PSMA-1-Pc413 is easily detectable at real-time imaging exposures (<67 ms) and can provide real-time IGS for urological surgeons (Supplementary Figs. S1 and S3; Supplementary Video S2). It was noticed that tumor depths obscured some GFP signal when imaged *in vivo,* but in all cases when tumors were excised, there was a good correlation between tumor GFP expression and PSMA-1-Pc413 fluorescence.

Surgery is the main treatment option for primary prostate cancer. In our novel approach, surgical resection was improved by PSMA-1-Pc413 IGS and, when immediately followed by PDT, significantly improved outcome. The combined approach resulted in a local tumor recurrence rate of only 1 of 8 animals, first detectable 80 days after completion of the

procedure, i.e., IGS+PDT (theranostic) cures prostate cancer 87.5% of the time. Cryo-image (Supplementary Fig. S2) of the tumor-bearing mice showed microdispersion of cancer cells away from the primary tumor mass, underscoring the prudence of the hypothesis and the importance of adjuvant PDT treatment. Pathology showed a good correlation between tumor remaining in the wound bed and tumor recurrence (Supplementary Fig. S5). IGS + PDT did not damage surrounding normal tissues. Pathology studies of resected tissues showed that the fluorescent tissue pieces resected during IGS were largely cancerous, achieving a sensitivity of 100% and specificity of 91.7%, respectively (Supplementary Table S1). It is unclear why the specificity was only 91.7%, given the selectivity of the PSMA-1-Pc413 molecules and the selective expression of the receptor. It is possible that the tissues that were false positive perhaps had significant background fluorescence due to occasional wounds inflicted on the animals by each other.

Even though PC3pip cells were engineered to overexpress the PSMA receptor, we used them for these studies because (i) they grow much more rapidly in mice than other prostate cancer cell lines and (ii) express levels of PSMA similar to many prostate cancer cells lines that have not been engineered to overexpress PSMA (Supplementary Fig. S7). We repeated studies with CWR22rv1 cells and demonstrated that the lower expression of PSMA in CWR22rv1 tumors does not significantly affect the utility of the approach to remove residual tumor tissue with PDT following surgery. Interestingly, the Western blot measurements of receptor levels suggest that lower PSMA levels on CWR22rv1 cells can still load cells with substantial level of the PSMA-1-PC413 molecule *in vivo*. More studies are underway to determine the reason(s) for these differences. Nevertheless, the lower levels of PSMA receptor levels are suitable for IGS+PDT approach. It has been reported recently that low-level PSMA expression is enough for tumor targeting and imaging (20), which supported our findings. Further, PSMA-1-Pc413 was able to detect LN metastases (Fig. 2). The application of IGS+PDT for removal of LNs, although beyond the scope of this study, has significant implications for successful outcomes and will be tested in the future, which include developing an immunocompetent PSMA-positive syngeneic cancer model to test the impact of the immune system on the IGS+PDT approach.

In conclusion, application of combined IGS and PDT technologies may be able to improve clinical treatment of prostate cancer for patients that elect to undergo radical prostatectomy. It will improve cancer tissue visualization and enable discrimination among cancerous, normal, neural, and muscle cells and tissues during surgery and has the ability to help visualize LN metastases. In particular, the PDT component of the developed theranostic probe provides an adjuvant therapeutic approach to destroy unresectable tissues and/or missed cancer cells, reducing the frequency of positive margins and cancer recurrence. The technology is novel, innovative, and has great potential to be translated into the clinic benefiting patients with prostate cancer but will require outcome studies in addition to decreasing positive tumor margins.

Supplementary Material

Refer to Web version on PubMed Central for supplementary material.

Acknowledgments

We thank Dr. Nancy Oleinick for advice on PDT treatment and National Foundation of Cancer Research for funding this research (J.P. Basilion).

The costs of publication of this article were defrayed in part by the payment of page charges. This article must therefore be hereby marked *advertisement* in accordance with 18 U.S.C. Section 1734 solely to indicate this fact.

References

1. Siegel RL, Miller KD, Jemal A. Cancer statistics, 2018. CA Cancer J Clin 2018;68: 7–30. [PubMed: 29313949]
2. Silberstein JL, Eastham JA. Significance and management of positive surgical margins at the time of radical prostatectomy. Indian J Urol 2014;30:423–8. [PubMed: 25378825]
3. Eastham JA, Kuroiwa K, Ohori M, Serio AM, Gorbonos A, Maru N, et al. Prognostic significance of location of positive margins in radical prostatectomy specimens. Urology 2007;70:965–9. [PubMed: 18068455]
4. Connolly JA, Shinohara K, Presti JC Jr., Carroll PR. Local recurrence after radical prostatectomy: characteristics in size, location, and relationship to prostate-specific antigen and surgical margins. Urology 1996;47:225–31. [PubMed: 8607239]
5. Vahrmeijer AL, Hutteman M, van der Vorst JR, van de Velde CJ, Frangioni JV. Image-guided cancer surgery using near-infrared fluorescence. Nat Rev Clin Oncol 2013;10:507–18. [PubMed: 23881033]
6. Mitra A, Khoo V. Adjuvant therapy after radical prostatectomy: clinical considerations. Surg Oncol 2009;18:247–54. [PubMed: 19285386]
7. Agostinis P, Berg K, Cengel KA, Foster TH, Girotti AW, Gollnick SO, et al. Photodynamic therapy of cancer: an update. CA Cancer J Clin 2011;61:250–81. [PubMed: 21617154]
8. Celli JP, Spring BQ, Rizvi I, Evans CL, Samkoe KS, Verma S, et al. Imaging and photodynamic therapy: mechanisms, monitoring, and optimization. Chem Rev 2010;110:2795–838. [PubMed: 20353192]
9. Muhanna N, Cui L, Chan H, Burgess L, Jin CS, MacDonald TD, et al. Multimodal image-guided surgical and photodynamic interventions in head and neck cancer: from primary tumor to metastatic drainage. Clin Cancer Res 2016;22:961–70. [PubMed: 26463705]
10. Kobayashi H, Choyke PL. Near-Infrared Photoimmunotherapy of Cancer. Acc Chem Res 2019;46:28–33.
11. Wang X, Tsui B, Ramamurthy G, Zhang P, Meyers J, Kenney ME, et al. Theranostic agents for photodynamic therapy of prostate cancer by targeting prostate-specific membrane antigen. Mol Cancer Ther 2016;15:1834–44. [PubMed: 27297866]
12. Eljamel MS, Goodman C, Moseley H. ALA and Photofrin fluorescence-guided resection and repetitive PDT in glioblastoma multiforme: a single centre Phase III randomised controlled trial. Lasers Med Sci 2008;23:361–7. [PubMed: 17926079]
13. Pogue BW, Rosenthal EL, Achilefu S, van Dam GM. Perspective review of what is needed for molecular-specific fluorescence-guided surgery. J Biomed Opt 2018; 23:1–9.
14. Wang X, Huang SS, Heston WD, Guo H, Wang BC, Basilion JP. Development of targeted near-infrared imaging agents for prostate cancer. Mol Cancer Ther 2014;13:2595–606. [PubMed: 25239933]
15. Prunty MC, Aung MH, Hanif AM, Allen RS, Chrenek MA, Boatright JH, et al. In vivo imaging of retinal oxidative stress using a reactive oxygen species-activated fluorescent probe. Invest Ophthalmol Vis Sci 2015;56:5862–70. [PubMed: 26348635]
16. AV DS, Lin H, Henderson ER, Samkoe KS, Pogue BW. Review of fluorescence guided surgery systems: identification of key performance capabilities beyond indocyanine green imaging. J Biomed Opt 2016;21:80901. [PubMed: 27533438]

17. Linxweiler J, Korbel C, Muller A, Hammer M, Veith C, Bohle RM, et al. A novel mouse model of human prostate cancer to study intraprostatic tumor growth and the development of lymph node metastases. Prostate 2018;78:664–75. [PubMed: 29572953]

18. Hiroshima Y, Maawy A, Zhang Y, Guzman MG, Heim R, Makings L, et al. Photoimmunotherapy inhibits tumor recurrence after surgical resection on a pancreatic cancer patient-derived orthotopic xenograft (PDOX) nude mouse model. Ann Surg Oncol 2015;22Suppl 3:S1469–74. [PubMed: 25893411]

19. Moore LS, de Boer E, Warram JM, Tucker MD, Carroll WR, Korb ML, et al. Photoimmunotherapy of residual disease after incomplete surgical resection in head and neck cancer models. Cancer Med 2016;5:1526–34. [PubMed: 27167827]

20. Nimmagadda S, Pullambhatla M, Chen Y, Parsana P, Lisok A, Chatterjee S, et al. Low-level endogenous PSMA expression in nonprostatic tumor xenografts is sufficient for in vivo tumor targeting and imaging. J Nucl Med 2018;59:486–93. [PubMed: 29025989]

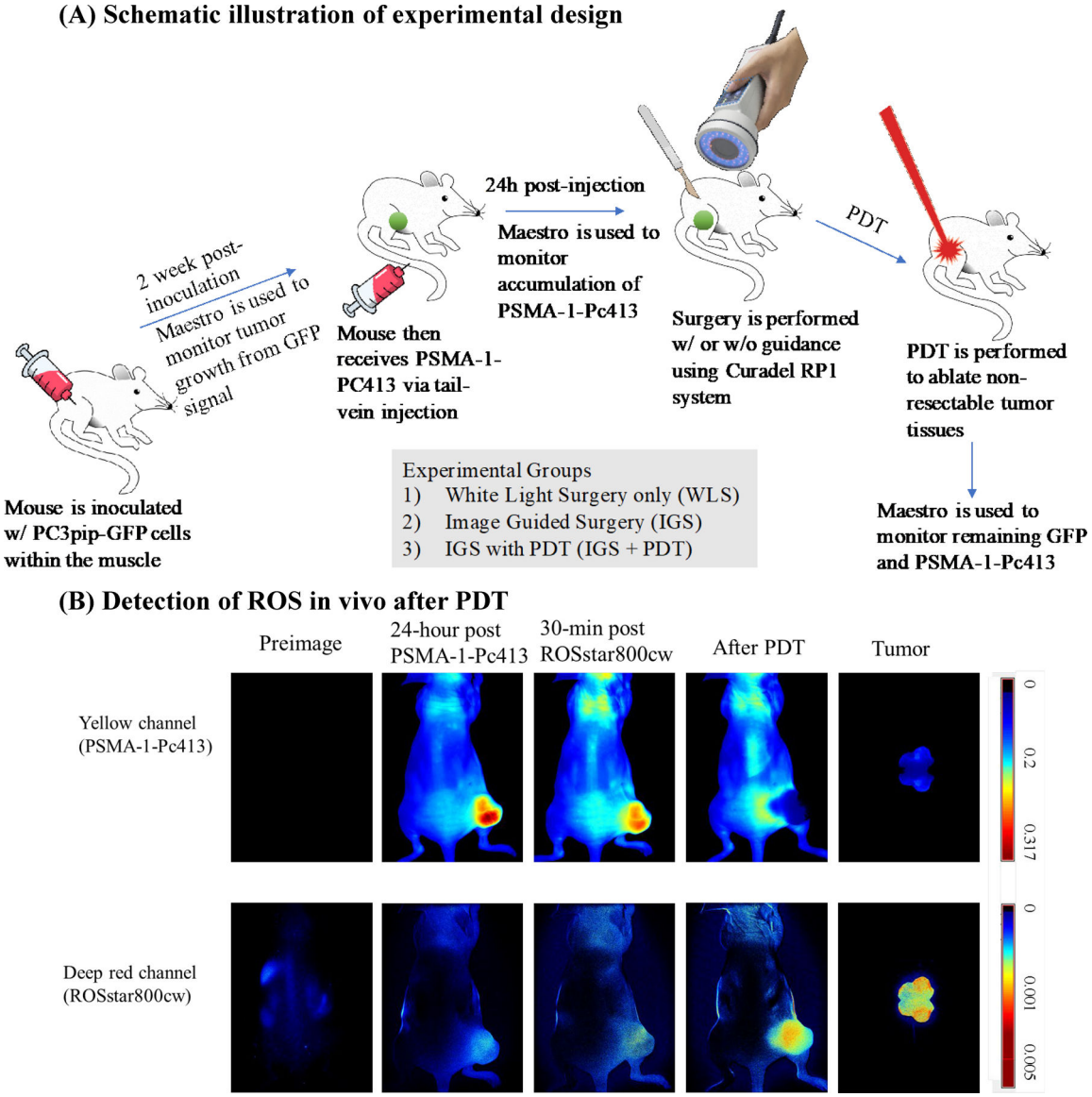

Figure 1.

Experimental design and generation of ROS *in vivo*. **A,** Scheme of experimental design. **B,** Detection of ROS *in vivo* after PDT. Mice bearing PC3pip tumor received PSMA-1-Pc413 and 24 hours later were administered ROSstar800cw, which detects ROS. Both PSMA-1-Pc413 and ROSstar800cw fluorescence were measured before and after light irradiation. Fluorescent signal in the deep red channel was observed after PDT, indicating generation of ROS after PDT.

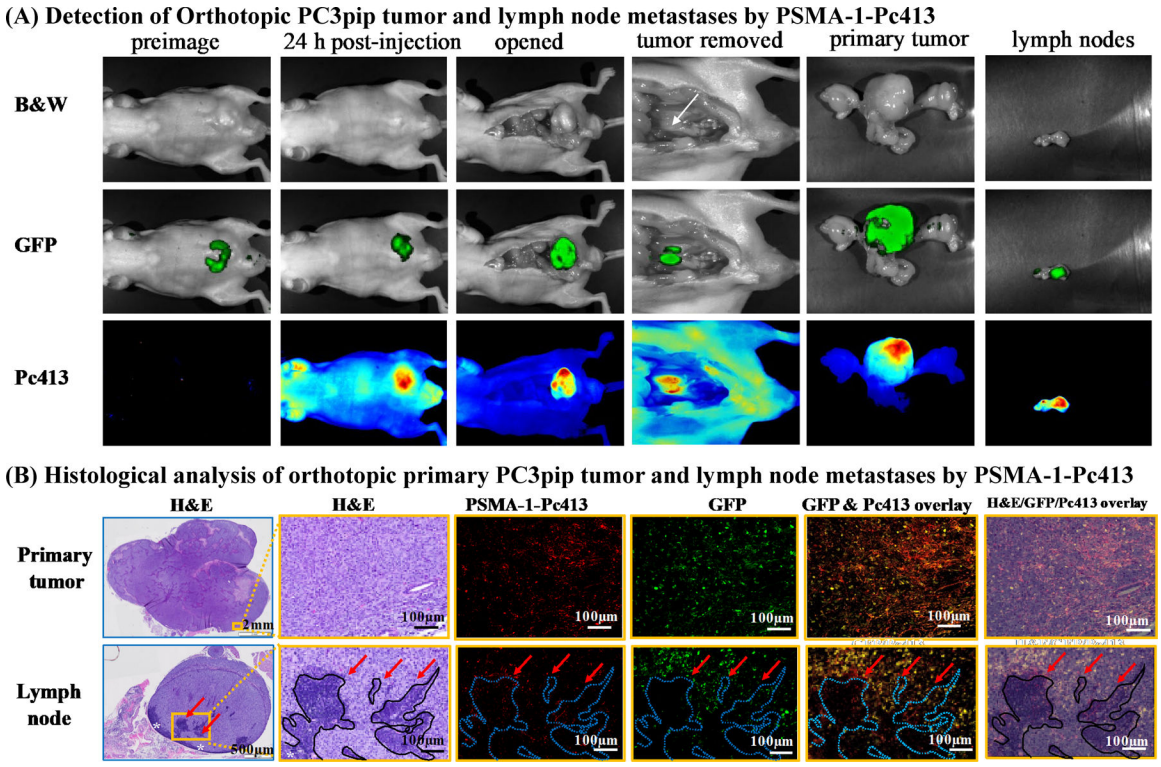

Figure 2.

In vivo fluorescence imaging of mice bearing orthotopic PC3pipGFP tumor. **A,** Representative images of whole mouse, primary tumor, and LNs. PSMA-1-Pc413 was able to detect both primary tumor and LN metastasis. White arrow, iliac LNs. Representative images are shown from five animals. **B,** Histologic analysis of resected primary tumor and LNs. Presence of tumor cells in LNs was confirmed by GFP signal (green), PSMA-1-Pc413 signal (red), and hematoxylin and eosin (H&E) staining. White asterisks (*), the rim of lymphocytes in LNs. Red arrows and dashed blue out lines indicate the residual lymphocyte islands in LN surrounded by tumor cells. Images in orange boxes are the enlarged microscopic images of the orange rectangles in column 1.

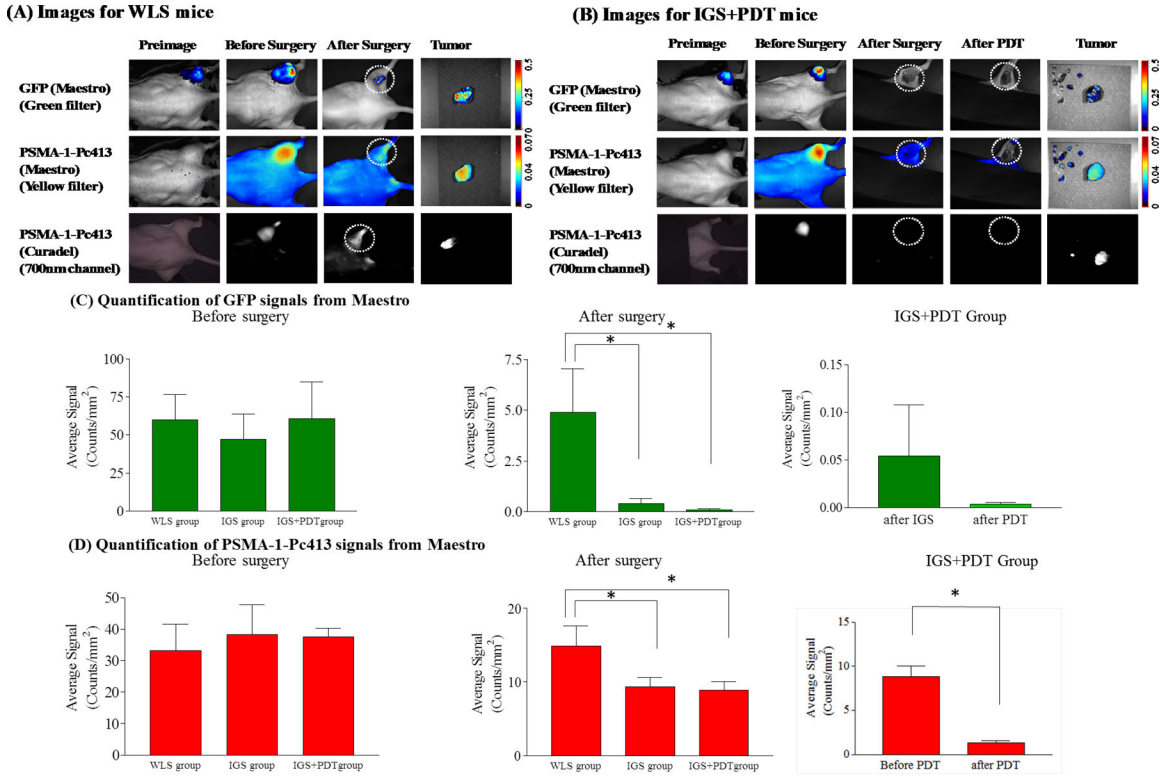

Figure 3.

Use of PSMA-1-Pc413 for IGS and PDT. **A,** Representative images of WLS mice under Maestro and Curadel imaging systems. Circles, surgical bed. **B,** Representative images of IGS+PDT mice under Maestro and Curadel imaging systems. Minimal amount of GFP and PSMA-1-Pc413 signals was observed in the wound with loss of PSMA-1-Pc413 signal due to photo activation. Circles, surgical bed. **C,** Quantification of GFP signals in the three experimental groups before surgery (left), after surgery (middle), and after IGS+PDT (right). Before surgery, similar GFP signal was observed in three experimental groups (left). After surgery, significantly lower GFP signal was observed in the IGS and IGS+PDT groups than in the WLS group (*, $P < 0.05$; middle). Values are mean±SD ($n = 5$ animals for WLS and IGS; $n = 8$ for IGS+PDT). **D,** Quantification of PSMA-1-Pc413 signals in the experimental groups before surgery (left), after surgery (middle), and after IGS+PDT (right). After surgery, a significant difference was observed between IGS/IGS+PDT and WLS group (middle; *, $P < 0.05$). Within the IGS+PDT group, PDT further reduced PSMA-1-Pc413 signal significantly as compared with after IGS alone (right). Values are mean ± SD ($n = 5$ for WLS and IGS, $n = 8$ for IGS+PDT).

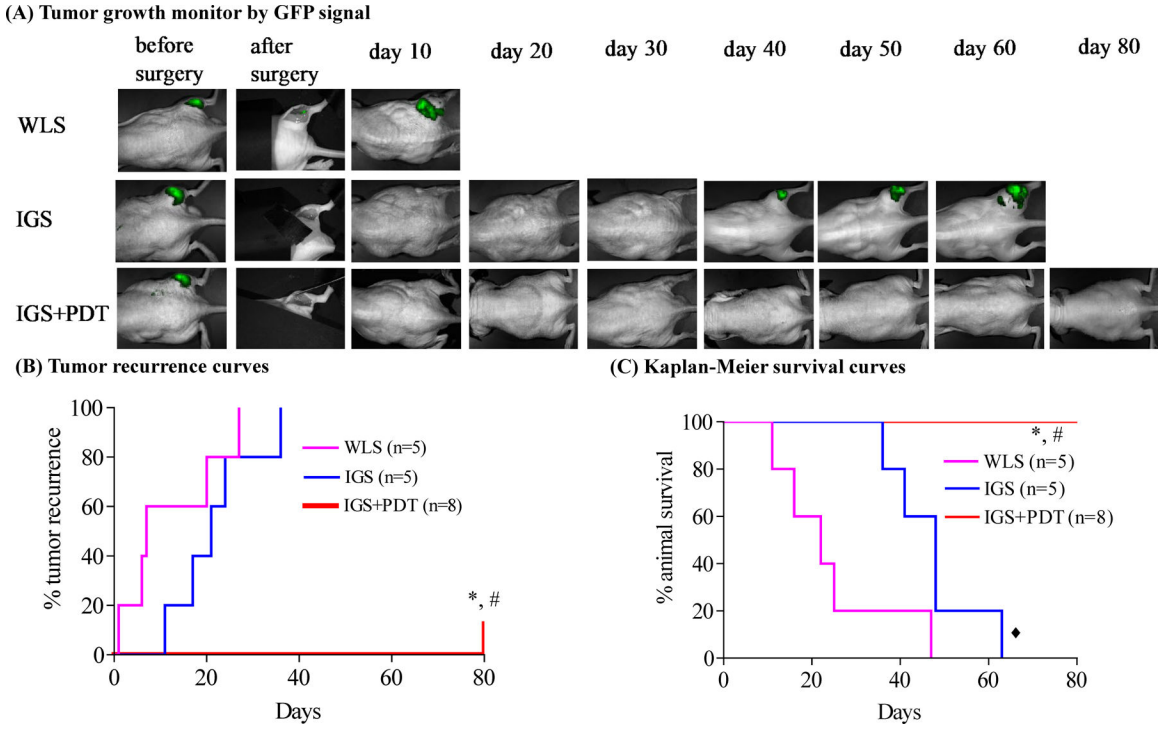

Figure 4.

Combination of IGS and PDT delayed tumor recurrence and extended animal survival. **A,** Representative postsurgery monitoring images of mice from WLS, IGS, and IGS+PDT groups measured using Maestro GFP channel. See Supplementary Fig. S6 for quantification of GFP signals. **B,** Tumor recurrence curves of mice from three experimental groups (n = animal numbers). IGS did not significantly delay tumor recurrence as compared with WLS (P = 0.2222). The tumor recurrence was significantly delayed by IGS+PDT. *, P = 0.0008, IGS+PDT vs. WLS; #, P = 0.00084, IGS+PDT vs. IGS. **C,** Kaplan–Meier survival curves of mice from the three experimental groups. IGS extended the animal survival significantly as compared with WLS (◆, P = 0.0317). The survival was further prolonged by PDT. *, P = 0.0008, IGS+PDT vs. WLS; #, P = 0.0008 IGS+PDT vs. IGS.